Biotribology 17 (2019) 19–29

Contents lists available at ScienceDirect

Biotribology

journal homepage: www.elsevier.com/locate/biotri

Modelling the evolution of electrochemical current in potentiostatic condition using an asperity-scale model of tribocorrosion

Ali Ghanbarzadeh*, Farnaz Motamen Salehi, Michael Bryant, Anne Neville

University of Leeds, School of Mechanical Engineering, Institute of Functional Surfaces, Leeds, UK

ARTICLE INFO

Keywords:
Tribocorrosion
Wear
Electrochemistry
Surface roughness

ABSTRACT

In this paper, an asperity-scale electrochemical model is combined with a computational contact mechanics solution to simulate a tribocorrosion system. The proposed approach is unique, considering the real-time evolution of surface topography, wear and corrosion. The proposed framework facilitates the prediction of wear, corrosion and its synergies by de-coupling wear and corrosion processes; better representing the physical and chemical system. The model is able to determine the current on the micro scale and the summation of the asperity currents is assumed to define the macro-scale quantity of the current. The evolution of current from this model has been validated with experiments using a ball-on-plate tribometer. The findings are in very good agreement with the experiments. The numerical model directly calculates the real area of contact in a tribocorrosive condition and highlights its importance in the electrochemical and mechanical wear. Investigating the effect of load also confirms that if the topography is evolved at different loading conditions, the electrochemical response of the system also evolves accordingly. After the model validation, the effect of mechanical wear on the corrosive wear has been computed and it suggests that the corrosive wear changes linearly with the mechanical wear.

1. Introduction

Metallic alloys are ubiquitous in aqueously lubricated tribological systems. This includes applications in automotive, aerospace, oil and gas, medical and food industries. Whilst the tribological systems vary significantly between these applications, one thing that unites all these applications is the fundamental degradation processes occurring at the tribological interfaces during sliding. Tribocorrosion describes the degradation process of a material whereby material is lost through combined mechanical (wear) and electrochemical (corrosion) processes. Whilst passive metallic alloys, such as stainless steels, CoCrMo and Ti-based alloys, are often employed because of their corrosion resistance, it is this characteristic which make these alloys susceptible to tribocorrosion. Passive alloys owe their corrosion resistance to the presence of a nano-metre thick passive oxide layer or passive film [1]. When such a material is subject to mechanical abrasion, the passive film can be damaged, partially or completely removed resulting in exposure of the metal to the corrosive environment. Due to the reactive nature of the underlying material, when the metal is exposed to the corrosive environment the surface will rapidly react with its environment to spontaneously reform the passive film. Whilst most studies assume that all metal ions released from the interface go directly into the formation of passive film, in reality a proportion of these will pass into the solution. Release of metal ions and particulates from a metallic surface has been implicated in the high profile metal hip recalls [2].

The complex dynamic process of combined material removal due to mechanical and electrochemical actions can lead to accelerated degradation of the material. In a tribocorrosion system, the overall measured wear is different from a simple summation of the electrochemical corrosion in the absence of mechanical rubbing and the mechanical wear in the absence of corrosive environment [3]. The tribocorrosive mechanisms were originally proposed by Uhlig and further expanded by Watson et al. [4]. The synergy equation, as described by Watson et al. and given in Eq. 1, demonstrates that material loss occurs from a combination of pure mechanical processes (V_m), pure corrosive processes (V_c) and their synergies where $\Delta V_{cw} + \Delta V_{wc}$ represent corrosion-enhanced wear and the wear-enhanced corrosion respectively [5].

$$V_T = V_m + V_c + \Delta V_{cw} + \Delta V_{wc} \quad (1)$$

The synergistic effects between corrosion and wear have been of particular interest and widely observed in abrasion [6–10], erosion [11–20] and sliding conditions [4,21,22]. Understanding the origins of material degradation in tribocorrosion contacts is critical prior to optimisation of such systems. The ability to predict and model the

* Corresponding author.
E-mail address: a.ghanbarzadeh@leeds.ac.uk (A. Ghanbarzadeh).

https://doi.org/10.1016/j.biotri.2019.02.003
Received 25 October 2018; Received in revised form 20 February 2019; Accepted 25 February 2019
Available online 26 February 2019

evolution of tribocorrosion has been the focus of many researchers [23–32]. Mischler and co-authors [25,28] developed mechanistic models of tribocorrosion. Corrosion was predicted by calculating the real area of contact in the whole wear track by linear interpolation of the wear track. Swaminathan and Gilbert [32] used mechanical models to calculate the real area of asperities in contact and showed that the abrasion rate of oxides is proportional to the product of real area and oxide thickness. They also presented that abrasion rate is related to asperity-asperity spacing. In other works, Stachowiak et al. [33,34] developed a multi-asperity contact mechanics model that can calculate the real area of contact and the corresponding current density. They have used the same model to develop the wear maps for tribocorrosion conditions [35]. Cao et al. [23] have developed a wear model for predicting material degradation in tribocorrosive environment considering the lubrication mechanism. They have combined an Archard-type mechanical material degradation model with an electrochemical Faraday-type wear model. The model used the calculated minimum film thickness to account for the effective load applied on the asperities. In some other works authors modelled the current response in a tribocorrosion experiment using high field conduction concepts [36,37]. They assumed that the current density is limited by the interface reaction and the growth of the oxide film occurs based on anodic polarization of the working electrode. In the most recent attempt, Nazir et al. [38] developed a novel approach to model synergistic wear-corrosion for nanocomposite coatings. They combined the nanomechanical properties of the coating with a stress-activated electrochemical model that was based on the Butler-Volmer equation [39]. They considered the evolution of the contact pressure and the corresponding evolution of the wear track.

There has been tremendous efforts in understanding the correlation between wear and corrosion in the tribology community as stated above. Different sophisticated experimental techniques have been developed [25,27] and numerous theories have been introduced [5,23,26,36]. However none of the models combine decoupled deterministic contact mechanics and corrosion models on the asperity scale. Literature lacks a unified coupled wear-corrosion model that integrates important physics of material degradation at the asperity level. The application of such models can be general and in any system that experiences synergistic effects of mechanical degradation and corrosion. Particular attention can be given to the biomedical field where the impact of tribocorrosive wear has shown to be significant especially in body joints and dentistry [40].

In a recent work, we have developed a novel framework for the prediction of wear, corrosion and its synergies occurring at tribological surfaces [41]. In this framework, a well-established electrochemical model has been integrated into an in-house developed transient contact mechanics and wear numerical framework [42], enabling a computationally efficient prediction of wear, corrosion and its synergies at the asperity scale. The contact mechanics model is capable of predicting wear and plastic deformation as well as surface topography evolution and simulation results were validated against experiments [43,44]. The tribocorrosion model is able to capture the microscopic and macroscopic electrochemical processes due to mechanical depassivation and mechanical wear. This manuscript presents the capability of the same tribocorrosion model in capturing the electrochemical current evolution in the dynamics of a tribocorrosion process. In this paper, we present a deterministic calculation for the evolution of the current in a sliding system. A brief explanation of the theory of the model is presented in Section 2 followed by results and discussions in Section 4.

2. Materials and Methods

2.1. Modelling Methodology and Theory

The model integrates two well-established mechanical and electrochemical models enabling the prediction of wear, corrosion and its synergies. The definitions of corrosion-enhanced wear and wear-enhanced corrosion are explained in detail in Ref [41]. The modelling framework has three main parts which will be described in detail in this section:

- Deterministic elasto-plastic contact mechanics simulation; The real area of contact will be calculated and the area of wear track will be calculated by tangentially moving the surfaces.
- Mechanical wear model; The transient mechanical wear model is applied at the asperity-level and modifies the geometry of the asperities and wear track area as a function of sliding distance.
- An electrochemical model; the electrochemical model is based on high field conduction re-passivation of a surface and is only valid for potentiostatic condition. Based on the exposed nascent surface area as a result of asperity contact, the resultant electrochemical current is calculated on the asperity-scale. Here we assume that the exposed computational surface nodes represent a unit area of totally depassivated material. The corresponding material loss due to corrosion is calculated based on the predicted current transient and used to further modify the tribological surfaces. This enables the wear enhanced corrosion and corrosion enhanced wear contributions to be determined.

The numerical procedure is plotted schematically in Fig. 1.

2.1.1. Contact Mechanics

Contact mechanics analysis is a necessity for calculating the area of contact and analysing wear. The contact model in this framework incorporates a Boundary Element Method (BEM) for the contact of rough surfaces. The model is an elastic-perfectly plastic model. In this approach hardness of the material is the criterion for limiting the contact pressure. The material hardness in the calculations is set to be the hardness of the softer material as it is reasonable to assume that the contact pressure will not exceed the hardness of softer material. A Fast Fourier Transform algorithm has been employed for the numerical efficiency. The details of the contact mechanics model can be found in the previous works of the authors [42,43]. It should be noted that only the effect of normal load has been considered in this work for simplicity. The effect of tangential loads can also be investigated in the future works. The measured surface topography of both surfaces is used as inputs of the contact mechanics solver. Two engineering rough surfaces (ball with the radius of 6 mm and a plate) are used for the simulations. An example of the contact mechanics of rough surfaces is shown in Fig. 2. The contact mechanics model is based on the complementary potential energy concept and the half space approximation is incorporated as the following:

$$\overline{u_z}(\mathrm{x},\mathrm{y}) = \frac{1}{\pi E^*}\int_0^L\int_0^L \frac{p(s_1,s_2)ds_1ds_2}{\sqrt{(s_1-x)^2+(s_2-y)^2}} \tag{2}$$

Where $\overline{u_z}(\mathrm{x},\mathrm{y})$ is the material deformation, $E^*$is the material composite elastic modulus calculated by $\frac{1}{E^*} = \frac{(1-\nu_1{}^2)}{E_1} + \frac{(1-\nu_2{}^2)}{E_2}$ where ν_1, ν_2, E_1 and E_2 are the Poisson's ratio and Elastic Modulus of material 1 and 2 respectively. $p(s_1,s_2)$ is the applied contact pressure. s_1, s_2 belong to the coordinates in which the load is applied and x,y belong to the coordinates in which the deformation is calculated. Then the problem will be solving the load balance and the surface deformation balance iteratively. The following set of equations must be satisfied:

$$\begin{Bmatrix} r = (Z_2(x,y) - Z_1(x,y)) + \overline{u_z}(\mathrm{x},\mathrm{y})\ \forall\ x,y \in A_c \\ p(x,y) > 0\ \forall\ x,y \in A_c \\ p(x,y) < H \\ \sum_{i,j=1}^{i,j=N} p_{i,j} = W \end{Bmatrix} \tag{3}$$

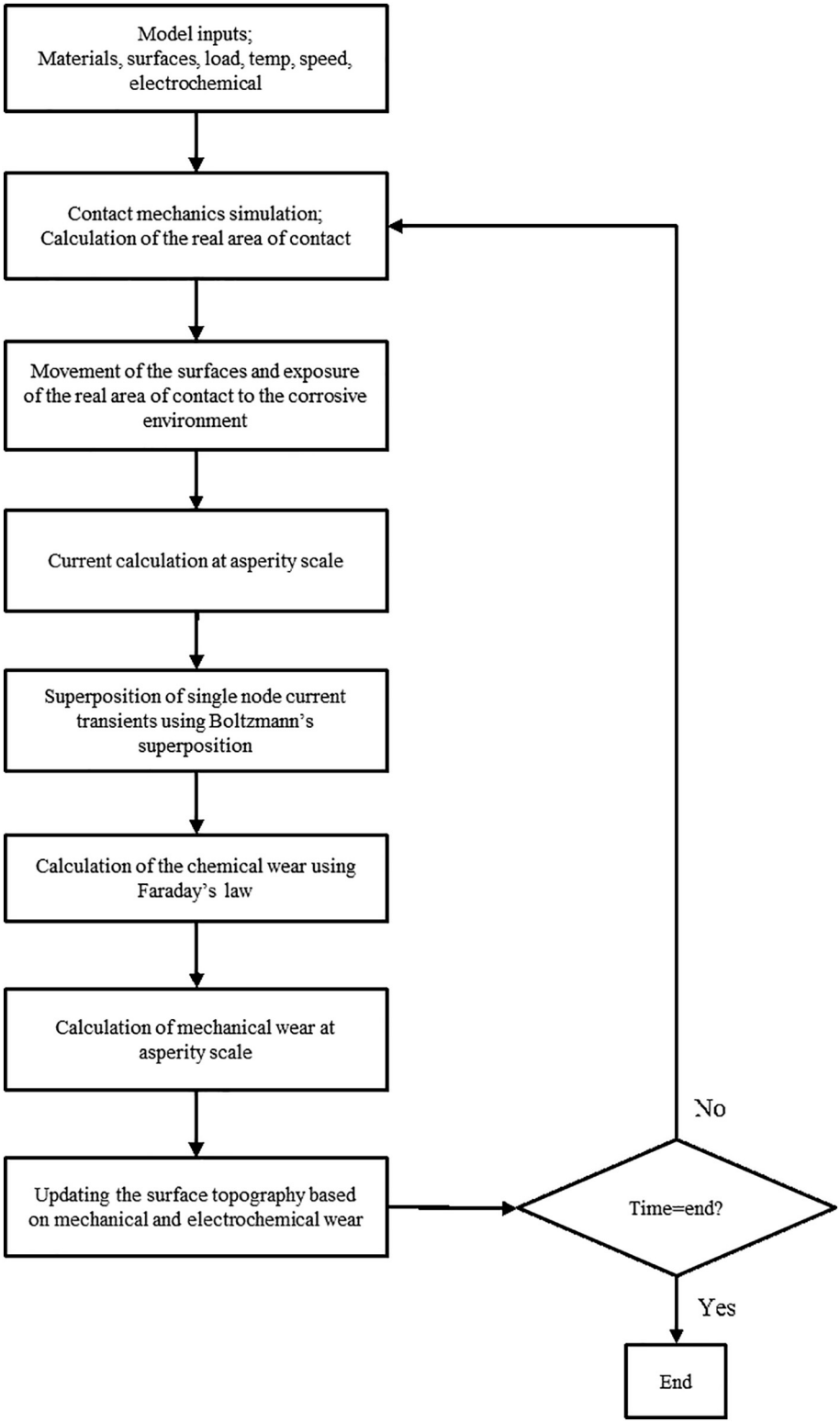

Fig. 1. Flowchart of the tribocorrosion model, showing how the evolution of the current can be captured deterministically

In which r is the rigid body movement of two rough surfaces, Z_2 and Z_1 are the surface profiles of the two rough surfaces and W is the total applied load. $A_c$is the area of contact, N is the total number of surface asperity nodes in the contact calculations and H is the material hardness.

Rough surfaces can move relative to each other and an asperity in one surface can experience contact with different asperities on the counter body due to its movement. Movement of surfaces can be simulated by shifting the matrix of numbers that contain values for surface node height (Z_1 and Z_2). This usually results in a wear track consisting of grooves being produced in the simulations.

2.1.2. Mechanical Wear Model

The mechanical wear model used in the current study is the

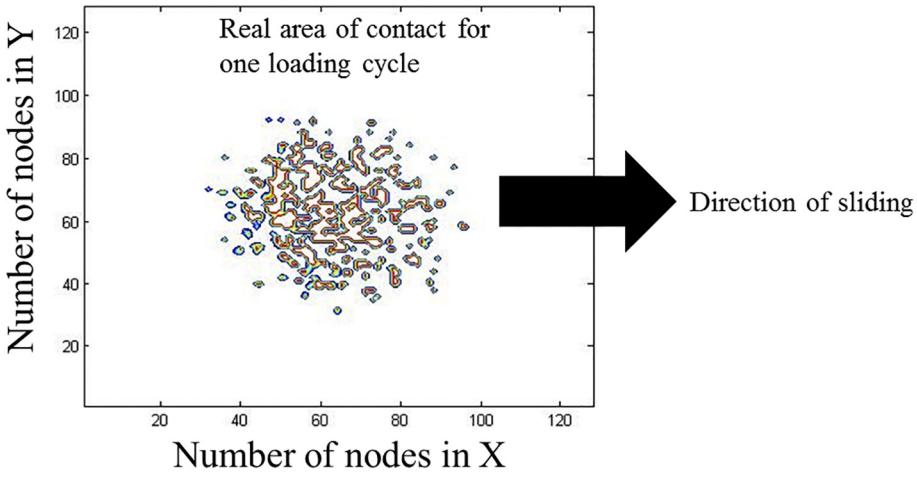

Fig. 2. Schematic representation of the contour of pressure in the contact mechanics model for real rough surfaces and calculation of the real area of contact for rough surfaces. The area is calculated for every loading cycle. The real area will evolve at every loading cycle during the sliding, due to tangential numerical movement of surfaces used in the contact model.

localized Archard's wear equation at asperity scale. The local mechanical wear depth can be calculated using Eq. 4:

$$\Delta h'(x,y) = \frac{K}{H}.\ P(x,y).\ \Delta t.\ v \tag{4}$$

where H is the material hardness, K is the dimensionless Archard's wear coefficient, P is the local contact pressure and v is the sliding speed. The values for P is calculated in each loading cycle based on the contact mechanics simulation. The values for other parameters (H, Δt and v) are obtained from the experiments and are reported in Tables 2 and 3. Both surfaces are prone to mechanical wear and only the hardness in Eq. 4 is different between two surfaces. The mechanical wear is calculated at asperity level and the height of surface nodes are modified.

2.1.3. Calibration of the Mechanical Wear

The experimentally measured wear reported in Section 3.1.2 is the material degradation due to combined electrochemical and mechanical processes. The electrochemical losses can be calculated by integrating the current over the whole period of the experiment and using the Faraday's law of Eq. 7. In order to obtain mechanical wear, the difference between total wear and the electrochemical wear will be calculated. It should be highlighted that the calculated difference does not represent the pure mechanical wear but rather the total mechanical wear. Total mechanical wear includes two components; pure mechanical wear and corrosion enhanced wear. A detailed discussion can be found in Ref [41]. This mechanical wear is then used to calibrate the wear model of Eq. 4. Archard's wear model of Eq. 4 is applied locally at asperity-scale. The K (dimensionless) value which defines the rate of wear is then calibrated using the experimental results and its value is 7×10^{-8}. K can be affected by all the physical and chemical parameters that affect the severity of the contact such as materials, lubricants and working conditions. Therefore a first principles prediction of it is not possible with the current knowledge. This calibration procedure is well-established in the literature [45,46].

2.1.4. Potentiostatic Electrochemical Model

In order to deterministically calculate the current response due to de-passivation and capture its effect on the surface topography evolution and wear, an electrochemical model should be applied at asperity level. A convenient and quick approach was to adapt a well-established macroscopic electrochemical model to the asperity level. The formulation to capture the current evolution is based on the assumption that film growth limits the interface reaction based on high field conduction [1] which was also adopted by other researchers [36,37]. The model assumes a film growth model with an anodic polarization controlled by means of a potentiostat and the current is formulated as the following:

$$i_{growth} = \frac{i^0_{growth}.\ e^{g^+U}}{1 + g^+.\ E_0.\ k_{film}.\ i^0_{growth}.\ e^{g^+U}.\ t} \tag{5}$$

where $i_{growth}{}^0$is the long-term growth current, $k_{film}$is the film growth kinetic rate and $g^+$is the generalized charge transfer factor formulated as:

$$g^+ = \frac{\alpha^+ F}{RT} \tag{6}$$

$\alpha^+$is the generalized charge transfer coefficient [47], F is the Faraday constant (96,485 ($^C/_{mol}$)), R is the ideal gas constant and T is the absolute temperature. U is the over potential and $U = U_{app} - E_{corr}$, E_0 is the electric field inside the film. $U_{app}$is the applied potential, $E_{corr}$is the natural corrosion potential and t is the time. In the case of tribocorrosion at open circuit potential, abrasion of the oxide layer will result in a shift in electrode potential, significantly affecting the rates and magnitude of corrosion currents evolved at the interface. Under this condition, the electrode potential is free to evolve with time along with the associated half-cell reactions. The current model does not consider such shifts and the corresponding changes in the electric fields at the interface.

In this model, the current increases significantly immediately after the contact and reduces gradually in time when the oxide layer is being formed (see Fig. 3) following the current transient of Eq. 5. It can be noted that the current transient of Eq. 5 is independent of mechanical parameters such as load and speed. The mechanical parameters will be affecting how the topography will evolve and will then eventually affect the macroscopic current. The calculated value from Eq. 5 gives the

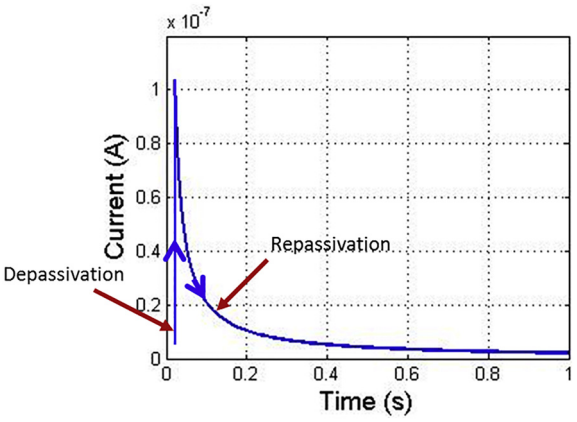

Fig. 3. Repassivation current profile for a single computational node in the model.

value of current and not the current density. The concept of current density will be meaningful if the total macroscopic current is divided by the area of contact which is not the case of simulations in this paper. However the current density can be calculated when the total macroscopic current is obtained and divided by the area of contact.

The value of the instantaneous increase in the current in the depassivation region is derived from the calibration of Eq. 5 at t = 0 and is equal to $i_{growth}{}^{0}.\ e^{g^{+}U}$. Therefore it will be a current transient on a single computational node. The area under the curve in Fig. 3 is then used to calculate the total charge transfer on the asperity level and the corresponding electrochemical loss is estimtaed using Faraday's law:

$$V_c = \frac{QM}{nF\rho} \tag{7}$$

V_c is the volumetric removal of material due to anodic reactions. Q, M, n, ρ and F are the total electric charge ($Q = \int_0{}^{t} i\ dt$), the atomic mass of the metal, the oxidation charge, the metal density and the Faraday's constant respectively. The n value for CoCrMo plate is 2.37 [29].

As with any computational model there are a number of simplifications that were made when compared to the actual physio-chemical system (explained in detail in Ref [41]). Like any other theoretical study, there are a number of limitations of this model. The electrochemistry model is based on assumptions of film growth limited by interface reaction. The electrochemical model is also based on the assumption that the working electrode is a net anode due to overpotentials. This means that the model is not able to study the conditions of a freely corroding electrode subjected to tribocorrosion. The fundaments of this model are based on the following points that are well established in the tribocorrosion literature. (i) The working electrode is sufficiently polarised in the anodic domain that cathodic half-cell reactions are negligible [27] and (ii) the measured and predicted currents from a metal surface undergoing tribocorrosion are at least an order of magnitude greater than the passivated metal surface. At this current time, the authors are not aware of any measurement or modelling techniques that enable the simultaneous quantification of open circuit potential and I_{corr} at a resolution sufficient to capture individual de/repassivation processes. The authors aim to make progress towards this current gap in the knowledge in the future and implement that in the robust numerical modelling of tribocorrosion.

2.1.5. Calibration of the Electrochemical Model

Calibration of the electrochemical model is an important part of this numerical framework. It is important for the model to accurately predict the current response in the dynamics of a sliding system. Surfaces will move relative to each and the number of computational nodes in contact in a quasi-static condition will change. This means that at every instance of sliding, there are possibly different number of contact spots and therefore a different contact area. In order to capture the electrochemical response, the current transients simulated on computational nodes will be superposed on eachother. Superposition of current profiles with different number of computational nodes at any instant results in a fluctutation in the current for one single sliding stroke. It should be noted that the superposition should consider the different timing of asperities coming into contact. Surfaces are moving relative to each other with speed V and this results in a time difference of $\frac{\Delta X}{V}$ for two adjacent computational nodes to come into contact; where ΔX is the size of the nodes used for relative movements. It means that the profile of current transients at every loading cycle will be superimposed with other loading cycles using a Boltzmann's superposition formula. The superimposition in one sliding stroke is shown schematically in Fig. 4 and the mathematical formulation is given here. It is important to notice that the depassivation of a single computational node has no kinetics. At the end of the stroke, the current decreases based on the repassivation kinetics explained in the electrochemical model.

The total current in every loading cycle can be calculated by finding the real area of contact and the number of unit computational nodes that are depassivated (N_i) using the following formula:

$$I_i(t) = N_i.\ i_{growth}(t) = N_i.\ \frac{i_{growth}^{0}.\ e^{g^{+}U}}{1 + g^{+}.\ E_0.\ k_{film}.\ i_{growth}^{0}.\ e^{g^{+}U}.\ t} \tag{8}$$

where $I_i$is the overal current in one loading cycle, $N_i$is the number of computational nodes that experience contact (depassivation) in one loading cycle (real area of contact) at ith time step. The current for one single sliding stroke can be formulated using a Boltzmann's superposition:

$$\begin{aligned} I_{stroke}(t) &= I_{(t-t_0)} + I_{(t-t_1)} + I_{(t-t_2)} + ...+I_{(t-t_M)} \\ &= (N_0.\ i_{growth}(t - t_0) + N_1.\ i_{growth}(t - t_1) + N_2.\ i_{growth}(t - t_2) \\ &\quad + ...+N_i.\ i_{growth}(t - t_i) + ...+N_M.\ i_{growth}(t - t_M) \end{aligned} \tag{9}$$

I_{stroke}(t) is the overall current response of the tribosystem in the duration of sliding, $N_0, \ldots, N_M$represent the number of computational surface nodes in contact and is calculated using the contact. This is achieved by calculating the number of non-zero elements in the contact pressure matrix. Since the real contact area is calculated for rough surfaces through a discretised contact model, the size of the computational nodes should be optimised [48] in order to get accurate results. The number of nodes in contact fluctuates considering the movement of surfaces in tangential direction. One can substitute $N_i$with $(\frac{F}{H})$ to calculate the real area of contact at every loading cycle. However in this paper, the real area of contact was calculated numerically for real engineering surfaces. $t_0, \ldots, t_M$ present the value of times at which different loading cycles occur due to the relative movement of surfaces. It means that the profile of one of the surfaces will be shifted in the sliding direction and new surface geometries come into contact. Every loading cycle in the simulation is assigned a time step and the value of time is calculated using the following equation:

$$t_i = (i).\ \frac{\Delta X}{V} \tag{10}$$

where ΔX is the lateral size of the computational nodes in the sliding direction, V is the sliding speed and i is the time step position. During the reciprocating motion, the value of the Boltzmann superposition time vary for different positions in the wear scar. This is because the sliding speed is different at different positions along the sliding direction. In this model, for simplicity, it is assumed that the asperities move with the same velocity all along the wear track. However, a greater repassivation time has been considered for the end of the stroke where the velocity of the contacting surfaces get to zero.

In order to calibrate the electrochemical model, the parameter $i_{growth}{}^{0}$ should be identified. This will be obtained by fitting Eq. 9 into the experimental results of current only for one sliding stroke. In this work, the measurements of one of the first sliding strokes is used to extract the parameters. The fitting parameter as well as the other parameters obtained from the literature (g^{+}, E_0 and k_{film}), are then used to predict the current for the rest of the simulation and to see the effect of real area of contact on the current evolution. The simulation results of the current for the first stroke and the corresponding experimental results used for the calibration are shown in Fig. 5. The experimental details of this measurement are given in Section 2.2.

It is interesting to see that the calculation of the current (blue line in Fig. 5) shows fluctuations due to the inhomogeneous nature of the surface roughness. When the upper surface (pin in our model) moves in the tangential direction, distribution and number of the asperities in contact change due to the random nature of asperity distribution. In the present paper the numerical data acquisition frequency ($2 \times 10^{3}\ s^{-1}$) is almost one order of magnitude larger than the experimental data acquisition rate ($100\ s^{-1}$). The trend of the simulation results of Fig. 5 are in good agreement with the trends shown in the literature [25,36,37]. The parameters used for the fitting are reported in Table 1.

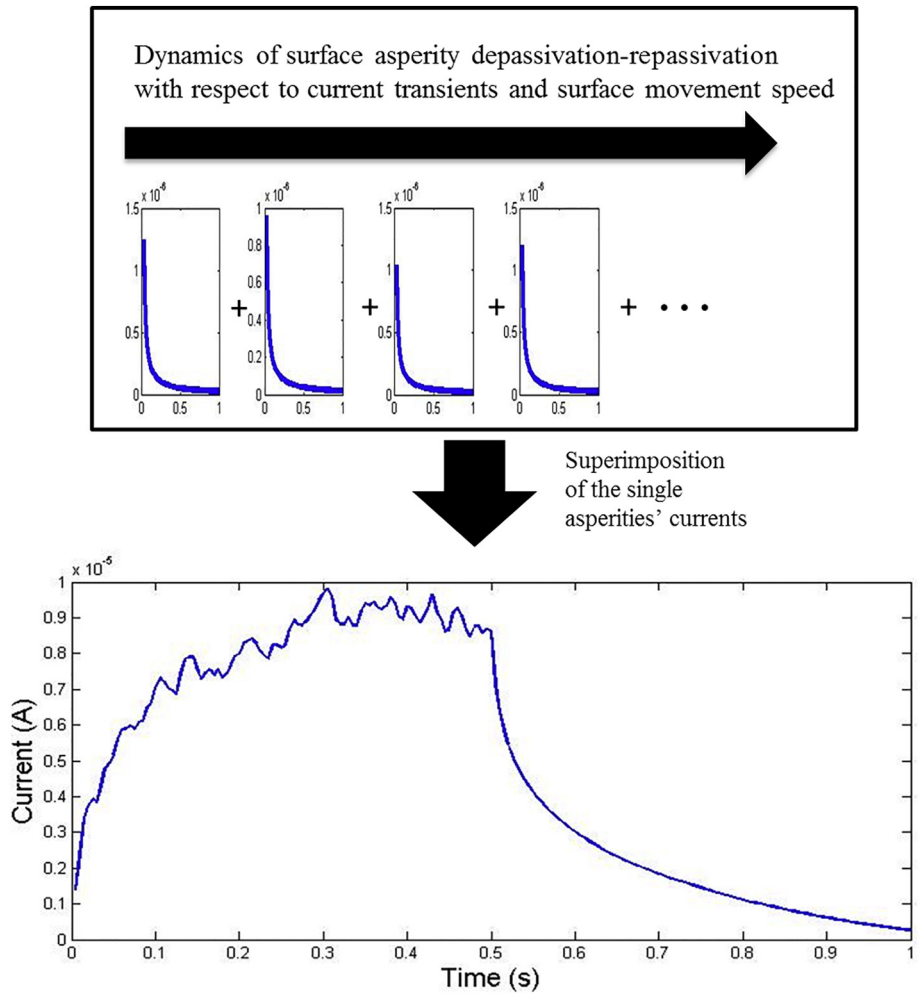

Fig. 4. Schematic of Boltzmann superimposition of the currents from single depassivated computational nodes in one sliding stroke.

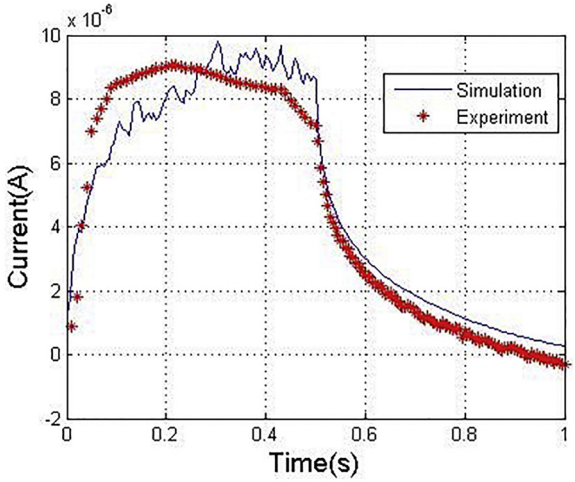

Fig. 5. Electrochemical current measured for the first stroke of sliding (0.5 S) is used to calibrate the electrochemistry model. An applied potential of 0 mV vs Ag/AgCl was applied (see Section 2.2). Simulation results are shown (blue line) as well as experimental data (red *). (For interpretation of the references to colour in this figure legend, the reader is referred to the web version of this article.)

Table 1
Parameters used in the electrochemistry model.

Parameters	Value
$i_{growth}{}^{0}$ (A)	10^{-9}
$g^{+}\left(1/V\right)$	18
$E_0\left(V/\mu m\right)$	500 [37]
$k_{film}\left(\mu m/A.s\right)$	5×10^{7}
U_{app} (V)	0

$i_{growth}{}^{0}$is the only electrochemical fitting parameter which is obtained from the experimental results. It should be noted that the applied potential is zero. The over potential (U) used in the model is the difference between applied potential (U_{app}) and the corrosion potential (E_{corr}). The corrosion potential in the experiments of CoCrMo with PBS solution was approximately −250 mV with respect to the Ag/AgCl reference electrode.

2.2. Experimental Methodology

2.2.1. Tribocorrosion Test Rig

A bespoke reciprocating ball-on-plate tribometer was used to simulate tribo-corrosion condition as shown in Fig. 6. A 12 mm diameter Si_3N_4 ball (R_a ~ 5 nm) was rubbed against a wrought low carbon CoCrMo plate (ø 25 × 6 mm, exposed surface area = 4.9 cm^2)

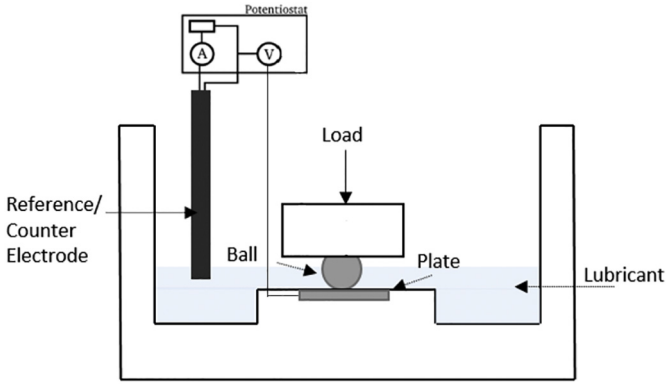

Fig. 6. The tribometer and the electrochemical cell attached to it [41].

Table 2
Testing conditions.

Parameters	Value
Load	5, 7.5, 10 N
Sliding amplitude	5 mm
Sliding velocity	20 mm/s
Test duration	1800 (1 ms dwell time)
Lubricant	Phosphate Buffered Saline (PBS) solution.

Table 3
Samples and material properties.

Parameters	Si_3N_4 ball	CoCrMo plate
R_q Roughness (nm)	5	20
Diameter (mm)	12	∞
Elastic Modulus (GPa)	310	210
Hardness (GPa)	25	4.5

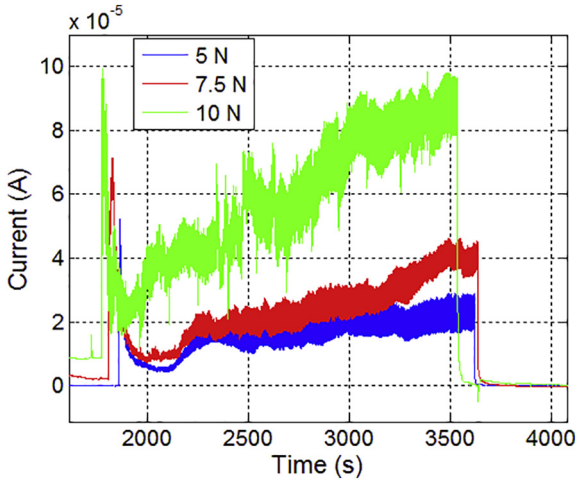

Fig. 7. Evolution of the current as a function of time for 3 applied loads of 5, 7.5 and 10 N [41].

according to the parameters outlined in Table 2. Prior to tribocorrosion, CoCrMo surfaces were polished to a surface roughness, (R_a) of approximately 20 nm. All surfaces were degreased using acetone and dried using a N_2 stream. The material specifications for both ball and the plate are presented in Table 3. A programmable moving coil actuator (SMAC, CA, USA) was used to displace the ball relative to the plate under a controlled saw-tooth, constant velocity profile. The normal load was realised through the application of a calibrated dead weight and varied from 5 to 10 N. A sliding amplitude of 10 mm at a velocity of 20 mm/sec.

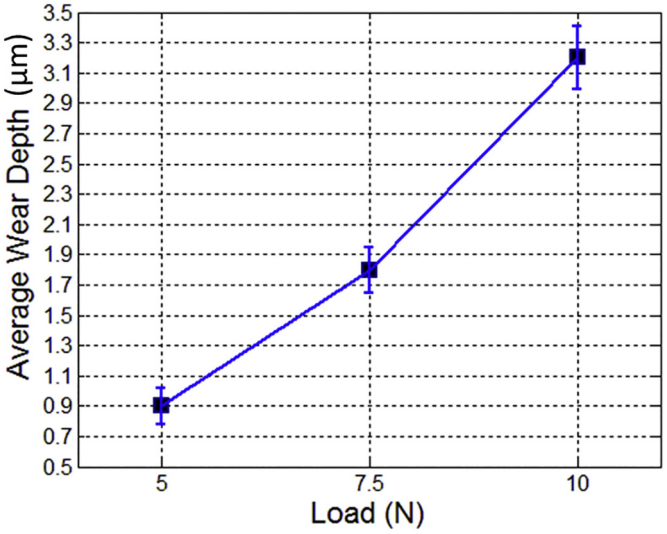

Fig. 8. Average depth of the wear tracks generated on a CoCrMo plates following testing in the tribometer with different loads.

In-situ corrosion measurements, were carried out using a 3-electrode electrochemical cell (also used in Ref [41]) which was integrated into the reciprocating ball-on-plate tribometer (see Fig. 6). To complete the electrochemical cell a combined Redox/ORP electrode (Thermo Fisher Scientific Inc., MA, USA) was used consisting of a Ag/AgCl reference electrode and Pt counter electrode. All tests were conducted under potentiostatic control using a computer controlled potentiostat (PGSTAT101, Metrohm Autolab B.V., Utrecht, Netherlands) and an applied potential of 0 mV vs Ag/AgCl. Surfaces were allowed to equilibrate for 1800 s before and after the application of sliding in order to observe de/re-passivation current transients, which were recorded at a rate of 100 Hz.

2.2.2. Surfaces Analysis

A White Light Interferometer (NPFLEX, Bruker, USA) was used in this work to analyse the profiles of the wear track after tribocorrosion tests. In this work, average wear depth of the wear track was measured for 5 different areas in the middle of the wear track and average values are reported.

Samples were then brought into a Scanning Electron Microscope (SEM, EVO MA15, Zeiss Oberkochen, Germany) to examine the morphology and investigate different possible wear modes. Results of the interferometry and SEM are reported in the experimental results section of this paper.

3. Results

3.1. Experimental Results

3.1.1. Electrochemical Current Transients

Fig. 7 (modified and reprinted from Ref [41]) shows the current trend over time of experiments at different loads. Over an initial static settle period, the plate is not subjected to wear and low current was observed. At the onset of sliding, there is a significant increase in current as evidenced in Fig. 7. This increase in current is due to the de-passivation of an area of the surface. During sliding, the current for all applied loads was observed to rise further as the test progressed. At the end of sliding, the current reduces and the sample surface repassivates as shown in Fig. 7. In addition, the increase in load caused increase in the current as shown in Fig. 7.

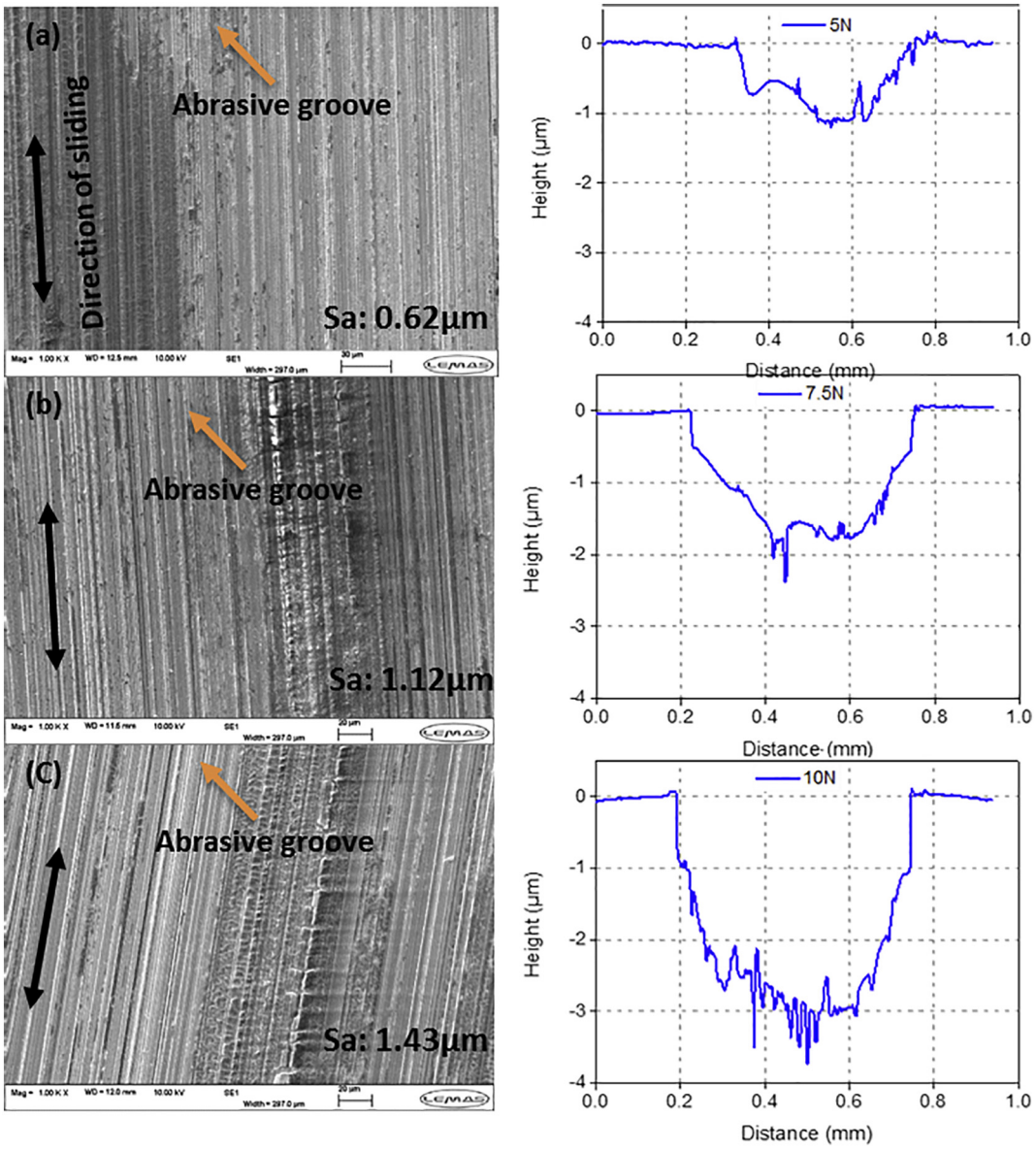

Fig. 9. 2D Depth profile across the wear scar of CoCrMo surfaces under different loads and SEM micrographs of the wear scars for the applied loads of (a) 5 N, (b) 7.5 N and (c) 10 N. (S_a is the arithmetical mean height of a line in 2D and is an extension of R_a).

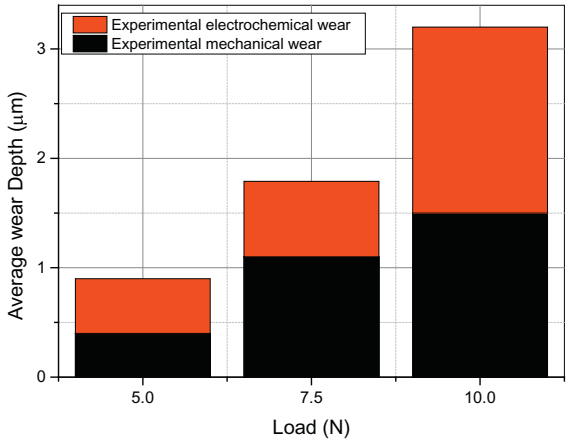

Fig. 10. Experimental electrochemical and mechanical wear for different loads.

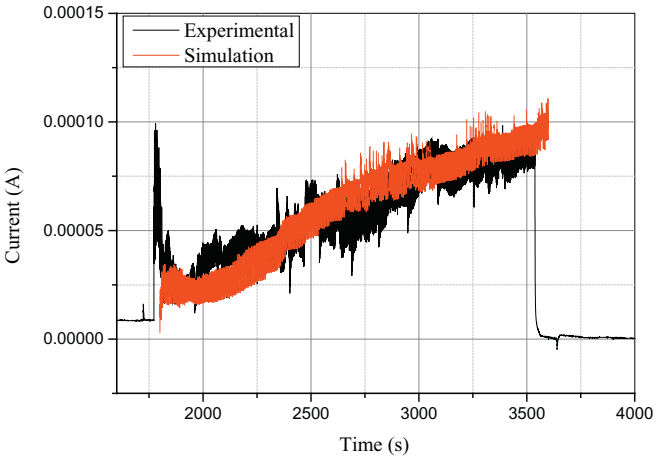

Fig. 11. Predicting electrochemistry during the 30 min experiment for 10 N load.

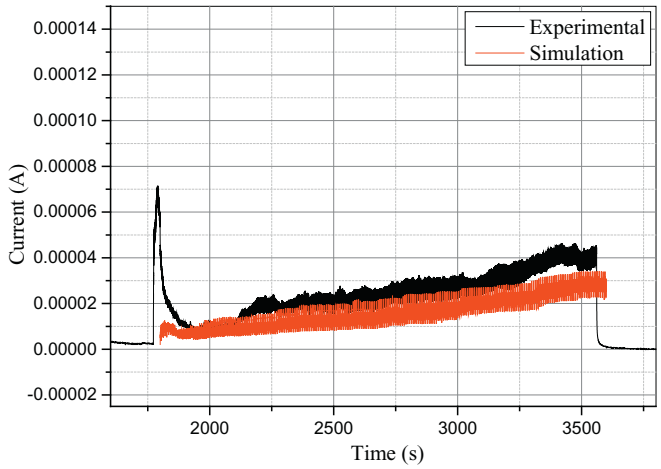

Fig. 12. Predicting electrochemistry during the 30 min experiment for 7.5 N load.

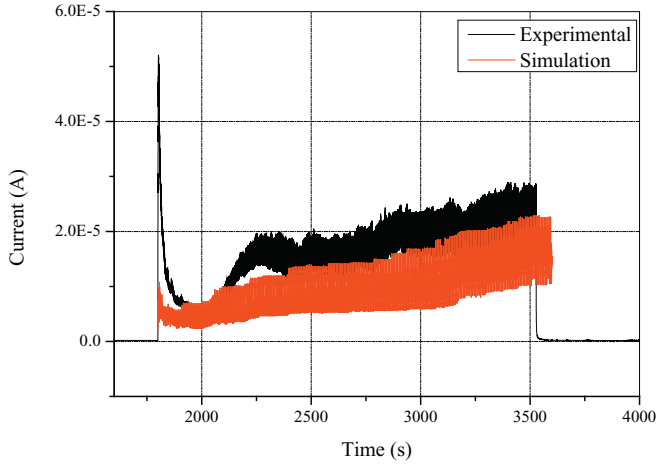

Fig. 13. Predicting electrochemistry during the 30 min experiment for 5 N load.

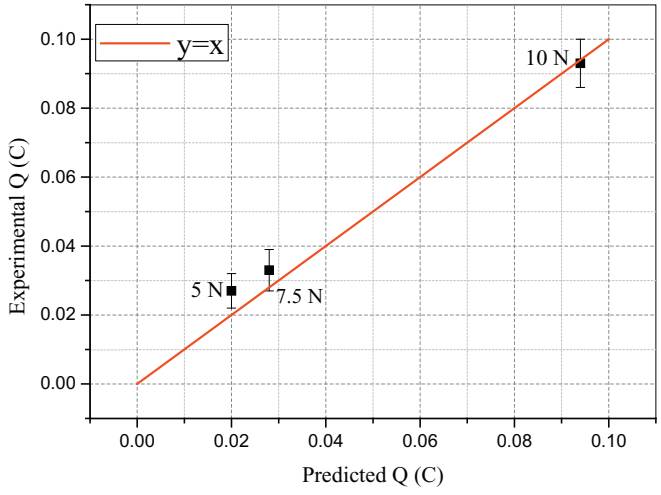

Fig. 14. Experimental Vs predicted total charge for applied loads of 5, 7.5 and 10 N and the variations from y = x line.

3.1.2. Total Material Loss

Fig. 8 demonstrates the average wear depth of samples tested in PBS applying various loads [41]. The results show that as the load increases, the wear depth increases as expected. In addition, it was observed that

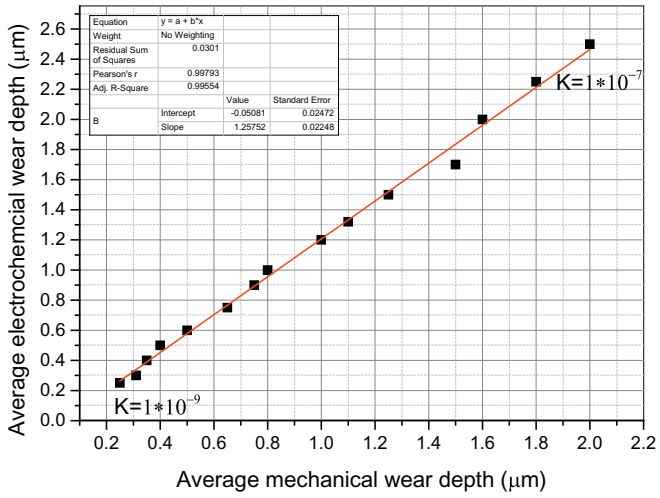

Fig. 15. The effect of mechanical wear on the electrochemical wear (simulation results).

the width of the wear scar in Y direction increased by applying higher load (Fig. 9). The electrochemical contribution of the material loss was calculated using the Faraday law and was subtracted from the total wear to calculate the mechanical wear. The results of mechanical and electrochemical wear for all three applied loads are presented in Fig. 10. It should be noted in Fig. 10 that V_{mech} (total mechanical wear) is equivalent to $V_m + \Delta V_{cw}$ and V_{chem} (total corrosive wear) is $V_c + \Delta V_{wc}$ and neither is strictly a mechanical (corrosion free) or chemical (mechanical free) damage. Later in this paper, the importance of the interplay between mechanical wear and corrosion is discussed.

SEM results and the wear micrographs show that there is a clear abrasive wear mechanism occurring on the surfaces for all three applied loads. It can be seen that the higher applied load results in bigger grooves to be formed on the wear track (Fig. 9a–c) which means a higher wear for higher applied load as expected. Analysis of the micrographs alongside the interferometry suggest that plate surface is rougher when worn at higher applied loads. This can be due to higher plastic deformation, higher wear and higher corrosion. Simulation results in the next section will confirm these observations.

3.2. Simulation Results and Discussion

3.2.1. Simulation of the Current

The depassivation area is dynamic, however, the real area of contact can be calculated in every load cycle and there is finite number of contact spots in the simulation. This results in the calculation of current in each time step. Fig. 11 shows the macroscopic measured current by incorporating local current densities on the contacting asperities of rough surfaces for the applied load of 10 N.

Fig. 11 shows that the current increases by time and it is because of the increase in the real area of contact due to the surface asperity conformity. The number of computational nodes in the contact with the counter body will increase with time due to flattening of surfaces. Therefore more nodes will be exposed to the corrosive environment caused by the movement of the surfaces.

It is important to see how the load affects the electrochemical response of a tribological system. It was shown by Maldonado et al. [26] that applied load changes the electrochemical response of a tribo-corrosion system. They clearly showed that higher loads induce higher current on the contacting surfaces. It is also reported in other works [25,28,36,29,49] that the mechanical action plays an important role in the chemical response of the surfaces by changing the area of contact and the area of depassivated nodes. The same electrochemical and mechanical parameters were used to predict the electrochemical

current for the applied loads of 7.5 N and 5 N and the simulation results are presented in Figs. 12 and 13 respectively.

The results in Fig. 12 show a good agreement of the simulation results with the experimental measurements. Fig. 13 also shows a good agreement in terms of the trend. However a slight divergence of the predicted electrochemical current from the measurements can be seen. The divergence of numerical and experimental results can be due to various reasons such as third-bodies, tribochemical effects, microstructural evolutions and consideration of constant sliding speed throughout the wear track.

Interpreting the results at different loads suggest that, the larger contact area due to the higher load results in more depassivation of the surface asperities and leads to a higher electrochemical current. This can be clearly seen from comparing the results of Figs. 11, 12 and 13.These results are in line with the experimental measurements of Maldonado et al. [26].

Although the current model has some simplification, the results in this section suggest that calculation of the real area of contact can result in fairly good prediction of the electrochemical current by implementing current growth at asperity-scale. The evolution of the real area of contact is also dependent on the applied load (see Ref [44]) and this will result in the current evolution during the time.

For comparison, the total measured experimental charge ($Q = \int_0^t i\,dt$) has been plotted versus the total predicted charge in the simulations as illustrated in Fig. 14. The variations of the scatter data from the y = x line represents the predictive capabilities of the model. It should be noted that this is not a fitting curve and just shows how prediction results are in-line with the experimental observations. The current results of Fig. 14 shows good agreement between experimental and the predicted values. This shows that the model is able to capture the total charge due to the tribocorrosion phenomena and hence is able to predict the local and overall electrochemical volumetric loss of the material.

3.2.2. Effect of Mechanical Wear on Corrosion

One capability of the current model is to investigate the interplay between the mechanical and the corrosive wear in a sliding condition. Although a thorough investigation into the interplay and the synergy effects has been carried out in our recent work [41], a brief example has been given here. It can be observed from the results that the electrochemical wear varies while the mechanical wear alters with the applied load. By varying the mechanical wear coefficient from 1×10^{-9}up to 1×10^{-7},the effect on the corrosive wear has been simulated. The rest of the simulation parameters are set unchanged as stated above and the load is 10 N. The electrochemical wear has been plotted for different values of mechanical wear and results are presented in Fig. 15. It is interesting to see that the corrosive wear linearly increases with the mechanical wear. This is due to the evolution of the contact area at different levels of mechanical wear which is an interesting finding. It shows that the increase in the mechanical wear rate, not only increases the mechanical wear, but also increases the corrosive wear. The increase in the real area of contact with the load has been presented in a recent work by Zugelj et al. [50]. They used an interferometer to experimentally capture the real area of contact and compared the results with analytical contact mechanics models. The proposed trend in Ref [50] is in agreement with the findings of the current papers and the fact that the real area of contact increases linearly with the applied load.

One advantage of the current approach is the direct calculation of the synergistic effects of corrosion on wear and wear on corrosion. The synergistic effect of corrosion on mechanical wear cannot be easily seen from the experimental studies of tribocorrosion therefore a mechanistic understanding of this effect is still not present in the literature. The current approach makes it possible to mechanistically model the corrosion-enhanced wear and the wear-enhanced corrosion.

4. Conclusions

In this work, a new deterministic approach is used to calculate the electrochemical current in a tribocorrosive wear environment. The novelty of the work lies in the coupled mechanical and corrosive wear at the asperity-scale. The predictions of the current in this situation lead to the following conclusions:

- Electrochemistry models can be applied on the asperity scale to calculate the micro-scale corrosive wear in deterministic approaches to gain more robust tribocorrosion predictive models.
- The hypothesis that electrochemical and mechanical wear occur at the same time is fairly a good assumption and further developments of their effects on each other and the synergy between them are the subject of ongoing research.
- Real area of contact is significantly important in the tribocorrosive wear environments and monitoring or predicting the area of contact can lead to a fairly good prediction of the current and thus the electrochemical wear of the system.
- It was shown that the model is able to predict the effect of load on the electrochemical response of the system and it is attributed to the different area of the contact corresponding to the applied loads.
- The topography evolution of the surfaces is captured via the model which result in the evolution of the real area of the contact. This feature is able to capture the evolution of the electrochemistry response of the system during the time.

References

[1] D. Landolt, S. Mischler, Tribocorrosion of Passive Metals and Coatings, Elsevier, 2011.
[2] A. Cobb, T. Schmalzreid, The clinical significance of metal ion release from cobalt-chromium metal-on-metal hip joint arthroplasty, Proc. Inst. Mech. Eng. H J. Eng. Med. 220 (2006) 385–398.
[3] R.J. Wood, Tribo-corrosion of coatings: a review, J. Phys. D. Appl. Phys. 40 (2007) 5502.
[4] S. Watson, F. Friedersdorf, B. Madsen, S. Cramer, Methods of measuring wear-corrosion synergism, Wear 181 (1995) 476–484.
[5] J. Jiang, M. Stack, A. Neville, Modelling the tribo-corrosion interaction in aqueous sliding conditions, Tribol. Int. 35 (2002) 669–679.
[6] D. Dunn, Metal removal mechanisms comprising wear in mineral processing, Wear Mater. 1985 (1985) 501–508.
[7] K. Barker, A. Ball, Synergistic abrasive—corrosive wear of chromium containing steels, Br. Corros. J. 24 (1989) 222–228.
[8] R. Noel, A. Ball, On the synergistic effects of abrasion and corrosion during wear, Wear 87 (1983) 351–361.
[9] A. Batchelor, G. Stachowiak, Predicting synergism between corrosion and abrasive wear, Wear 123 (1988) 281–291.
[10] D. Kotlyar, C. Pitt, M. Wadsworth, Simultaneous corrosion and abrasion measurements under grinding conditions, Corrosion 44 (1988) 221–228.
[11] V. De Souza, A. Neville, Corrosion and erosion damage mechanisms during erosion–corrosion of WC–Co–Cr cermet coatings, Wear 255 (2003) 146–156.
[12] H. Meng, X. Hu, A. Neville, A systematic erosion–corrosion study of two stainless steels in marine conditions via experimental design, Wear 263 (2007) 355–362.
[13] A. Neville, M. Reyes, H. Xu, Examining corrosion effects and corrosion/erosion interactions on metallic materials in aqueous slurries, Tribol. Int. 35 (2002) 643–650.
[14] S. Shrestha, T. Hodgkiess, A. Neville, Erosion–corrosion behaviour of high-velocity oxy-fuel Ni–Cr–Mo–Si–B coatings under high-velocity seawater jet impingement, Wear 259 (2005) 208–218.
[15] V. Souza, A. Neville, Corrosion and synergy in a WC Co Cr HVOF thermal spray coating—understanding their role in erosion–corrosion degradation, Wear 259 (2005) 171–180.
[16] R.J. Wood, Erosion–corrosion interactions and their effect on marine and offshore materials, Wear 261 (2006) 1012–1023.
[17] B.W. Madsen, Measurement of erosion-corrosion synergism with a slurry wear test apparatus, Wear 123 (1988) 127–142.
[18] A. Neville, T. Hodgkiess, J. Dallas, A study of the erosion-corrosion behaviour of engineering steels for marine pumping applications, Wear 186 (1995) 497–507.
[19] A. Neville, T. Hodgkiess, H. Xu, An electrochemical and microstructural assessment of erosion–corrosion of cast iron, Wear 233 (1999) 523–534.
[20] T. Hodgkiess, A. Neville, S. Shrestha, Electrochemical and mechanical interactions during erosion–corrosion of a high-velocity oxy-fuel coating and a stainless steel, Wear 233 (1999) 623–634.
[21] S. Watson, B. Madsen, S. Cramer, Wear-corrosion study of white cast irons, Wear 181 (1995) 469–475.
[22] X. Jiang, S. Li, D. Tao, J. Yang, Accelerative effect of wear on corrosion of high-alloy

stainless steel, Corrosion 49 (1993) 836–841.
[23] S. Cao, S.G. Maldonado, S. Mischler, Tribocorrosion of passive metals in the mixed lubrication regime: theoretical model and application to metal-on-metal artificial hip joints, Wear 324 (2015) 55–63.
[24] S. Guadalupe, S. Cao, M. Cantoni, W.-J. Chitty, C. Falcand, S. Mischler, Applicability of a recently proposed tribocorrosion model to CoCr alloys with different carbides content, Wear 376 (2017) 203–211.
[25] D. Landolt, S. Mischler, M. Stemp, Electrochemical methods in tribocorrosion: a critical appraisal, Electrochim. Acta 46 (2001) 3913–3929.
[26] S.G. Maldonado, S. Mischler, M. Cantoni, W.-J. Chitty, C. Falcand, D. Hertz, Mechanical and chemical mechanisms in the tribocorrosion of a Stellite type alloy, Wear 308 (2013) 213–221.
[27] S. Mischler, Triboelectrochemical techniques and interpretation methods in tribocorrosion: a comparative evaluation, Tribol. Int. 41 (2008) 573–583.
[28] S. Mischler, S. Debaud, D. Landolt, Wear-accelerated corrosion of passive metals in tribocorrosion systems, J. Electrochem. Soc. 145 (1998) 750–758.
[29] S. Mischler, A.I. Munoz, Wear of CoCrMo alloys used in metal-on-metal hip joints: a tribocorrosion appraisal, Wear 297 (2013) 1081–1094.
[30] J.L. Gilbert, S.A. Mali, Y. Liu, Area-dependent impedance-based voltage shifts during tribocorrosion of Ti-6Al-4V biomaterials: theory and experiment, Surf. Topogr. 4 (2016) 034002.
[31] J.R. Goldberg, J.L. Gilbert, Electrochemical response of CoCrMo to high-speed fracture of its metal oxide using an electrochemical scratch test method, J. Biomed. Mater. Res. Part A 37 (1997) 421–431.
[32] V. Swaminathan, J.L. Gilbert, Fretting corrosion of CoCrMo and Ti6Al4V interfaces, Biomaterials 33 (2012) 5487–5503.
[33] A. Stachowiak, W. Zwierzycki, Analysis of the tribocorrosion mechanisms in a pin-on-plate combination on the example of AISI304 steel, Wear 294 (2012) 277–285.
[34] A. Stachowiak, W. Zwierzycki, Tribocorrosion modeling of stainless steel in a sliding pair of pin-on-plate type, Tribol. Int. 44 (2011) 1216–1224.
[35] A. Stachowiak, P. Tyczewski, W. Zwierzycki, The application of wear maps for analyzing the results of research into tribocorrosion, Wear 352 (2016) 146–154.
[36] P. Jemmely, S. Mischler, D. Landolt, Electrochemical modeling of passivation phenomena in tribocorrosion, Wear 237 (2000) 63–76.
[37] C.-O. Olsson, M. Stemp, Modelling the transient current from two rubbing electrode configurations: insulating pin on metal substrate and metal pin on insulating substrate, Electrochim. Acta 49 (2004) 2145–2154.
[38] H. Nazir, Z.A. Khan, A. Saeed, A. Siddaiah, P. Menezes, Synergistic wear-corrosion analysis and modelling of nanocomposite coatings, Tribol. Int. 121 (2018) 30–44.
[39] E.M. Gutman, Mechanochemistry of Materials, Cambridge Int Science Publishing, 1998.
[40] M. Mathew, P. Srinivasa Pai, R. Pourzal, A. Fischer, M. Wimmer, Significance of tribocorrosion in biomedical applications: overview and current status, Adv. Tribol. 2009 (2009).
[41] A. Ghanbarzadeh, F.M. Salehi, M. Bryant, A. Neville, A new asperity-scale mechanistic model of tribocorrosive wear: synergistic effects of mechanical wear and corrosion, J. Tribol. 141 (2019) 021601.
[42] A. Ghanbarzadeh, M. Wilson, A. Morina, D. Dowson, A. Neville, Development of a new mechano-chemical model in boundary lubrication, Tribol. Int. 93 (2016) 573–582.
[43] A. Ghanbarzadeh, P. Parsaeian, A. Morina, M.C. Wilson, M.C. van Eijk, I. Nedelcu, D. Dowson, A. Neville, A semi-deterministic Wear model considering the effect of zinc Dialkyl Dithiophosphate Tribofilm, Tribol. Lett. 61 (2016) 1–15.
[44] A. Ghanbarzadeh, E. Piras, I. Nedelcu, V. Brizmer, M.C.T. Wilson, A. Morina, D. Dowson, A. Neville, Zinc Dialkyl Dithiophosphate Antiwear Tribofilm and its effect on the topography evolution of surfaces: a numerical and experimental study, Wear 362-363 (2016) 186–198.
[45] J. Andersson, R. Larsson, A. Almqvist, M. Grahn, I. Minami, Semi-deterministic chemo-mechanical model of boundary lubrication, Faraday Discuss. 156 (2012) 343–360.
[46] J. Andersson, A. Almqvist, R. Larsson, Numerical simulation of a wear experiment, Wear 271 (2011) 2947–2952.
[47] K. Vetter, F. Gorn, Kinetics of layer formation and corrosion processes of passive iron in acid solutions, Electrochim. Acta 18 (1973) 321–326.
[48] B.N. Persson, Contact mechanics for randomly rough surfaces, Surf. Sci. Rep. 61 (2006) 201–227.
[49] M. Stemp, S. Mischler, D. Landolt, The effect of mechanical and electrochemical parameters on the tribocorrosion rate of stainless steel in sulphuric acid, Wear 255 (2003) 466–475.
[50] B.B. Zugelj, M. Kalin, Submicron-scale experimental and theoretical analyses of multi-asperity contacts with different roughnesses, Tribol. Int. 119 (2017) 667–671.